Journal of Advances and Scholarly Researches in Allied Education
Vol. 16, Issue No. 6, May-2019, ISSN 2230-7540

Magnetic Properties of Nano Zinc Ferrite by VSM

Mohammad Suhel[1]* Dr. Satish Kumar[2]

[1] Research Scholar, Department of Physics, Sri Satya Sai University of Technology & Medical Sciences, Sehore, M.P., Sehore

[2] Research Guide, Department of Physics, Sri Satya Sai University of Technology & Medical Sciences, Sehore, M.P., Sehore

Abstract – In the present investigation, studying the effect of transition metal ions substitution in tuning magnetic and dielectric properties of the synthesized materials are the main tasks. A literature review on ferrite samples provides the information about the chronological developments in lower temperature preparation methods, ecofriendly approaches, easily scalable to industry requirements and forecasting the suitability of these samples for the possible applications. The important scientific information/ findings were reported on transition metals or the rare earth elements doped mixed ferrites. In the present research, undoped and transition metal/s like Cr3+, Ni2+ and Cu2+ doped ZFs have been chosen to synthesize by three wet chemical methods such as solution combustion (SCS) with ODH as fuel, plant latex mediated combustion or green combustion synthesis (GCS) and hydrothermal (HYDS) routes. In GCS method, the extract from fresh leaves of Mimosa pudica (MP) was selected as a fuel for the preparation of ZFs. The synthesized materials were characterized by advanced materials characterization tools such as XRD, SEM, TEM, FTIR, PCS, UV-Visible spectroscopy, PL, XPS and TG/DSC analysis. To know the magnetic interactions in the prepared samples, the magnetic measurements were carried out at room temperature (RT) (for all samples) and below RT (for only undoped ZFs) using vibrating sample magnetometer, VSM 7410.

Key Words – Nanomaterials, Zinc Ferrites, Magnetic Properties, Mimosa Plant

----------X----------

1. INTRODUCTION

Nanomaterials

Research into a variety of chemical, mechanical and physical properties is the basis for a glimmer of understanding how this interplay manifests itself in gaining control over the creation of matter. NMs are generally, NPs of metals, semiconductors, dielectrics, magnetic materials or organic compounds and polymers. NMs constitute a regime in which the energy is in between the bulk material and the molecules / atoms. The NMs manifest for exceptionally fascinating and useful properties. In NMs, large fraction of atoms on the surface of the material; high surface energy; spatial confinement and reduced numbers of imperfections that makes these materials as special.

There is a noteworthy change in the properties of NMs as related to their bulk complement. NMs display new phenomenon associated with the quantized effects and with the predominance of surfaces and interfaces. The finite size of the particle limits the spatial distribution of the electrons which leads to the quantized energy states. The quantum confinement has applications in optoelectronic and photonics field [1-3].

The space charge contribution from the increased surface to volume ratio enhances the electrical conductivity of nanosized conducting ceramics. When materials size reduces to nanoscale, there is a significant decrease in crystallite volume which alters the electronic structure from continuous electronic bands to discrete or quantized electronic levels. Therefore, in nanoregime, the continuous optical transitions between the electronic bands become discrete and the properties of NMs become size dependent. Domain dependent magnetic and transport characteristics alter significantly at nanoscale. The reduction in particle size enhances self-diffusion, solute diffusion and solute solubility in NMs attributed to defective atomic coordination at the grain boundaries of the nanocrystals. The higher fraction of the grain boundaries results in higher values of specific heat capacities than its bulk. Due to a reduction in size

www.ignited.in

of less than < 5 nm, an increase in the energy band gap between the valence and the conduction bands results in a blue shift in its optical absorption properties [4, 5].

Magnetic NMs exhibit size-dependent property due to the large surface-to- volume ratio. A different local environment for the surface atoms in their magnetic coupling with the neighboring atoms leads to the different surface magnetic properties. Single magnetic domain concept in nanoregime shows super-paramagnetism, in which the magnetization is randomly distributed and aligns only under the applied magnetic field and immediate disappearance of magnetization with respect to the external field. This particular property helps in increasing the limit of storage devices, color imaging, ferro-fluids, magnetic refrigeration etc. To understand the physicochemical and optoelectronic properties of the NMs and to exploit them for commercial applications, it is important to account for the unique properties of NMs. It is imperative to understand the interface characteristics, structural, magnetic and transport properties of these materials.

Ferrites are having low eddy current losses with high resistivity of the order 10^{11} cm compared to 10^{7} cm of iron, low dielectric losses, high saturation magnetization, high permeability and moderate permittivity.

Ferrites were used in many applications such as radio receivers to increase the sensitivity and selectivity, used as cores in audio and TV transformers, used in digital computers and data processing circuits, used to produce low frequency ultrasonic waves by magnetostriction principle, used in non-reciprocal microwave devices like gyrator, isolator and circulator, used in power limiting and harmonic gyration devices, used as magnetic shift register, hard ferrites were used in permanent magnets which in turn used in instruments like galvanometers, ammeter, voltmeter, flux meters, speedometers, watt meters, compasses and recorders. The clean fuel, i.e. hydrogen can be produced by electrolysis or thermal decomposition in the temperature range of 1073–1273 K using ferrite-based Nano composites. Ozonation, photooxidation, adsorption, membrane filtration and flocculation were used to extract colorants and contaminants from wastewater used for nanoferrites. For the reutilization of waste water in industry, the combination of magnetic NPs like ferrites with photocatalysis is the attractive method.

2. REVIEW OF LITERATURE

Many ferrite characteristics are interdependent upon different material aspects. To put these issues under one umbrella, the different synthesis methods, compositions and cation distributions recorded in the literature survey of transition metals doped nanocrystalline zinc ferrite (ZF), diverged structural parameters, various morphological factors, crystallite / particle sizes obtained, magnetic parameters which governs the magnetic interactions with in the material, dielectric parameters and activation energy, optical energy band gaps and their reported applications were considered. The best efforts are made to concise the important results at one place, especially for the chronologically ordered transition metals doped and undoped nano zinc ferrite powders.

Research to develop the materials of desired magnetic materials which are suited for high frequency operation was started seriously at around 1930's. In 1945 Snoek discussed in detail the basic fundamentals of physics and technology of practical ferrite materials. In 1948, the Neel theory of ferromagnetic provided the theoretical understanding of these types of materials. It was proposed that the magnetic properties depends upon cation distribution among the A and B sites. Negative exchange interaction exists among A-A, B-B and A-B sites. For dominant A-A and B-B exchange interactions, the materials remain paramagnetic at lowest temperature. In 1950s, due to new applications such as electronic media, computer, microwave devices and communication ferrite materials took lead. Among the many noteworthy soft ferrites few are zinc ferrite (ZF), Nickel ferrite (NF), copper ferrite (CuF), NiZn ferrites (NiZnF), Mn-Mg ferrites (MnMgF) and Mn-Zn ferrites (MnZnF) as soft ferrites and barium and strontium ferrites as hard ferrites. In 1952, Hogan [6] studied the microwave ferrite devices. In 1956 Hastings et al [7] showed the antiferromagnetic transition in ZF using neutron powder diffraction method. In their paper, the particles size was in the μm range. They showed that the compound undergoes transition from paramagnetic to antiferromagnetic at ~ 9 K. Based on the line intensities they proposed the cell edge variation and antiferromagnetic alternation of ferromagnetic bands.

Yafet [8] studied antiferromagnetism in ferrites. He extended the Neel theory and showed realignment of sub-lattices in opposite directions to each other leading to ferrimagnetism. Uitert [9] reported dc resistivity of Ni-ZF prepared by solid state reaction method. The loss of zinc in Ni-ZF at high temperature is expected to introduce Fe^{2+} ions. Small amount of Fe^{2+} addition made the samples with high conductivity. Kedem [10] showed the Yafet-Kittel type of ordering in Ni-ferrite. Koops [11] reported the fall of dielectric constant and resistivity of the Ni0.4Zn0.6Fe2O4 ferrites. Rowen et al [12] reported the sharp decrease of tanδ with increase in specific resistance. The Y-K angles of Zn1-xNixFe2O4 ferrites were reported by Murthy [13]. The non-collinear Y-K type of magnetic ordering was increased with Zn contents and decreased with increasing temperature. NiFe2O4 showed the Neel type ordering which was independent of temperature. The spin pinning at

www.ignited.in

ferrite-organic interfaces was reported by Berkowitz [14]. In Ni-Ferrite coated with organic molecules showed large angles with external magnetic field of 68.5 KOe, whereas for uncoated Ni-Ferrite such variation was not exhibited. V2O5 doped Ni-Ferrite were prepared by solid state reaction by Jain [15]. The electrical conductivity was observed at 0.4 mol % of V2O5 content, this was due to solubility limit of V2O5 in the spinel lattice. Curie temperature and Y-K angles of Cu substituted Ni-ZF were reported by Joshi. Non-collinear spin arrangement was observed in all the samples due to the presence of Y-K angles. The decrease in A-B interaction was due to increased Y-K angles attributed to lower the Curie temperature (Tc) of the samples. Due to smaller magnetic moment of Cu, there is a decrease in Ms and Tc with addition of Cu to Ni-ZF.

3. EXPERIMENTAL TECHNIQUES

Different methods for the synthesis of NPs were reported depending on the material of interest, the properties and applications dependent on their size. There are two wider synthesis areas, namely physical and chemical methods. The broadly used physical method is a solid state reaction in which structural degradation or grosser grain structures result from the use of high mechanical energy.

In chemical methods, solution based chemical reaction are generally used to improve homogeneity, purity and also to reduce particle size called as wet chemical methods. Among the chemical methods, sol-gel technique is common, where starting materials are soluble, highly dispersed metal alkoxides or soluble salts in the molecule level and fixing the dispersion state in a gel by the hydrolysis and condensation reaction leads to the formation NPs. In contrast, the solution combustion, green combustion and hydrothermal methods chosen in this thesis, have many advantages. SCS arises as a promising technique for nanopowder preparation.

NMs preparation by green chemistry routes has received much attention as it was clean, non-toxic, eco-friendly, lowering the reaction temperature, helps in obtaining the special structures and free from unwanted by products. Hence the use of plant latex for the extraction of NPs is one of the important methods of preparation. This method of preparation is named as GCS method.

3.1 Materials Used

Table 3.1 provides the information about the list of chemicals used in the present work. All the samples were of analytical or equivalent grade without further purified.

Table. 3.1. List of chemicals/solvents used for the synthesis of ferrites and zinc oxide

Sl. No.	Chemical Name	Chemical Formula
1	Zinc nitrate	$Zn(NO_3)_2.6H_2O$
2	Ferric Nitrate	$Fe(NO_3)_3.9H_2O$
3	Chromium oxide	Cr_2O_3
4	Nickel Nitrate	$Ni(NO_3)_2.6H_2O$
5	Copper Nitrate	$Cu(NO_3)_2.6H_2O$
6	Silver conductive paste	Ag
7	Ethanol	C_2H_5OH
8	Sodium hydroxide	NaOH
9	Nitric acid	HNO_3
10	Distilled water	H_2O

The selection procedure for the dopants (chromium, nickel and copper) into the parent compound (Zinc ferrite – ZnFe2O4) and their quantity were chosen according to the crystal field theory. Based on these analysis, Cr^{3+} varied in a small quantity of mol % as ZnCrxFe(2-x) O4 (x= 0.01, 0.03, 0.05, 0.07), whereas Ni^{2+} and Cu^{2+} were varied with mol % of (x = 0.1, 0.3, 0.5 and 0.7) in NixZn(1-x)Fe2O4/CuxZn(1-x)Fe2O4.

3.2 Methods of Synthesis

Synthesis of nanoferrites can be skilled in two ways namely, chemical and physical methods. Various routes are being pursued under chemical processes, such as colloidal, capping, cluster forming, sol-gel, electrochemical, auto combustion, micro emulsions, etc. Physical approaches commonly used include epitaxial molecular laser, ionized cluster stream, the origins of liquid metal ions, sputtering and monomer gas aggregation. The goal in all of these preparation methods is to limit the particle size to where the particle size is less than the twice Bohr excitation radii. The next objective is to minimize particle agglomeration and repetitiveness of the experimental results.

3. 4 Oxalyl Dihydrazide Fuel Preparation

Fuels are the source of carbon and hydrogen, which on combustion form simple gaseous molecules of CO_2 and H_2O and liberate heat.

In the SCS method, the fuel used was Oxalyl Dihydrazide ($C_2H_6N_4O_2$, ODH) prepared freshly for undoped and doped zinc nitrate. ODH is prepared in the way suggested by Patil et al. 146.14 g of 1 mol of diethyl oxalate was added drop wise to 100.12 g of 2 mol of hydrazine hydrate and dissolved in 225 ml of double distilled water. A white precipitate obtained was allowed to stand overnight then washed with ethanol, filtered and dried in open atmosphere. The reaction of the process is as below:

$$(COOC_2H5)_2 + 2N_2H4.H_2O \rightarrow (CON_2H_3)_2 + 2C_2H_5OH + 2H_2O \quad \ldots (3.1)$$

3.5 Evaluation of Stoichiometric

The stoichiometry for SCS is calculated based on the total oxidizing (O) and reduction (F) valentia of the oxidizer and the fuel, maintaining unity of the O / F ratio[45]. Oxidizing elements have positive valencies and negative valencies of the decreasing elements. The gross oxidizing valence of metal nitrates can be determined by mathematical summation of oxidizing components and removal of oxidizing valences. Similarly, the total reducing valency of a reducer (fuel) can be obtained by arithmetic summation of oxidizing and reducing valencies of elements present in the fuel. Carbon, hydrogen were treated as reducing elements with corresponding values + 4, + 1 and oxygen was treated as an oxidizing element with a value of -2. Thanks to their conversion to molecular nitrogen during combustion, nitrogen valence was known to be zero.

$$\text{Oxidizer/fuel ratio} = \frac{x\sum \text{all oxidizing valency of oxdizer}}{(-1)\,y\sum \text{reducing valency of fuel}} \quad \ldots\ldots\ldots\ldots\ldots\ldots(3.2)$$

Where x is the number of moles of oxidizer and y is the moles of fuel required

$$x = \frac{\text{weight of metal nitrate taken for preparation } (W_x)}{\text{Molecular weight of nitrate } (M_x)}$$

$$\text{And } y = \frac{\text{weight of fuel to be added for preparation } (W_y)}{\text{Molecular weight of fuel } (M_y)}$$

The total valencies of metal nitrates by arithmetic summation of oxidizing and reducing valencies was – 15, this means that metal nitrates were strong oxidizers. The calculated valence of ODH ($C_2H_6N_4O_2$) was +10. The O/F ratio was calculated based on oxidizing [O] and fuel [F] valencies of the reactants, keeping O/F = 1. By keeping O/F = 1, the amount of heat liberated is maximum.

3. 6 Extraction of *Mimosa Pudica* Plant as a Fuel

NMs preparation using diverse biological entities has been received attention in the last two decades due to cost effective, eco-friendly, energy efficient and non- toxic methods [148, 149]. In GCS method of synthesis, the *Mimosa pudica* (M.P.) leaves extract was selected as a fuel. Fresh leaves of M.P. were collected and washed thoroughly many times with tap water and double distilled water. After that the healthy leaves were air-dried using sterile blotter paper under shade for 15 – 20 days at room temperature (RT). Next the sample was pulverized using sterile electric blender the obtained fine powder was stored in sterile polyethylene bags before its use. The sample was subjected to successive solvent extraction using 1L thimble and soxhlet apparatus. Furthermore, the deionized water was refluxed successively for 72 h. Fig. 3.1 shows the picture of M.P. and the Soxhlet apparatus used.

In both SCS and GSC methods, the approximate yield estimated was in the range of 18 – 24%.

Fig. 3.1 Leaves of *Mimosa pudica* plant

3.8 Zinc Ferrite Samples Preparation by SCS (Solution Combustion Synthesis) Method

The flow charts for the general procedure of SCS method and the specific method of preparation of ZF selected using ODH or using M.P. leaves extract were shown in Fig.3.2. ZF with stoichiometric composition was prepared by SCS method. Mixtures of zinc nitrate (MERCK), iron (III) nitrate (MERCK) and freshly prepared ODH / M.P. were taken in a crystalline dish. The reactants were dissolved in about 25 ml of double distilled water and were stirred with magnetic stirrer for thirty minutes. The chemical reaction of synthesis process is represented by

$$Zn(NO_3)_2.6H_2O\,(aq) + 2Fe(NO3)_3.9H_2O\,(aq) + 4C_2H6N4O_2(aq)/\text{ M.P. extract (aq)} \rightarrow ZnFe_2O_4\,(s) + 36\,H_2O\,(g) + 12\,N_2\,(g) + 8\,CO_2\,(g) \quad (3.4)$$

For the doped samples, part of zinc nitrate and iron nitrate quantities was replaced by the equivalent stoichiometric quantities of dopant metal nitrates or metal oxides. In the case of chromium ions incorporation, freshly prepared chromium nitrate was obtained from chromium (III) oxide and concentrated nitric acid as precursors and oxalyldihydrazide / MP leaves extract as a fuel were diluted with distilled water and subjected to low temperature combustion. In other cases, direct metal nitrates were selected and the repetition of the complete process is same as mentioned above.

The active ingredients of M P leaves is polysaccharides of carbohydrades and flavonoids etc. They shows affinity towards water and incorporates strongly the metal ions into the biological structures. When metal nitrates mixed with M P gel type solution, the cations gets distributed and forms complex three dimensional polymeric network called egg box structure and the explanation about the same as egg-box model. The resulting polymeric network undergo slow

decomposition when subjected to heat treatment and prevent the strong agglomeration. The schematic representation of 5,7,3', 4' - tetrahydroxyl-6-C-beta-D-glucopyranosyl flavonoid network in trapping the zinc ferrite nanoparticles is shown in Fig. 3.2.

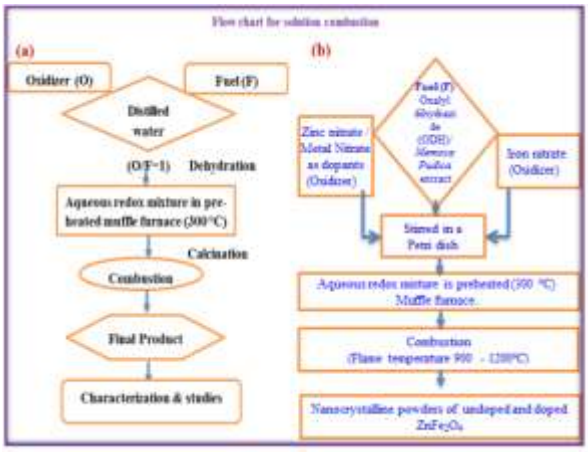

Fig. 3.2 (a) Basic flowchart of SCS and GCS methods and (b) specific method of SCS preparation adopted in the present work.

3.9 Hydrothermal (HYDS) Method

This method involves heating of metal salts, oxides or hydroxides as a solution or suspension in water or an organic solvent at controlled temperature and pressure for a known time in an air tight system called autoclave. Typically, the temperature in a hydrothermal process falls between the boiling point of water and critical temperature (Tc = 374 °C), while the pressure is about 100 K pa. The product obtained is washed by distilled water or acetone to get rid of ions and other impurities. After drying in air, fresh well-dispersed oxides NPs are obtained.

3.10 Characterization Methods Used

The synthesized materials were characterized by advanced materials characterization tools.

- Powder X-ray diffraction (XRD) analysis was performed using Shimadzu 7000 / Philips analytical X-ray diffractometer with CuK radiation of wavelength 1.5406 Å. The data was collected in range from 10 - 80 degree with the scan rate of 0.02/0.033 degree.s^{-1}.
- The Fourier transform infrared (FTIR) spectra were collected in absorption mode using the Perkin Elmer spectrometer (Spectrum 1000) and the KBr pellets.
- Scanning electron microscope (SEM) has studied the morphology of the prepared sample {TM 3000 / Zeol /JEOL (JSM-840A)} images. The composition analysis of the sample was carried out using EDX attached with SEM.
- TEM analysis was carried out using JEOL JEM 2100 with accelerating voltage up to 200 kV LaB6 filament.
- Photon correlation spectroscopy (*PCS*) or particle size distribution was performed using dynamic light scattering technique with zetasizer 6.20. Before PCS study the samples were dispersed in water medium using sonicator for about two minutes.

4. MEASUREMENT OF MAGNETIC PROPERTIES OF DOPED AND UNDOPED NANO ZINC FERRITE BY VSM

Zinc ferrite (ZF) is a ceramic material, which shows paramagnetic behaviour in its bulk form due to its normal spinel structure, with Zn ions incorporation almost exclusively at A-sites. Once processed as nanoparticles, it becomes ferrimagnetic owing to a partial movement of Zn ions to the B-sites. Due to non- magnetic substitution, intra-sublattice interaction becomes comparable with inter-sublattice interaction. In such a case chaos and agitation arises in the spin subsystem due to the specific magnetic structures; ferrimagnetic order, local spin canting, antiferrimagentic order, re-entrant spin glass (RSG) and spin glass etc.. The magnetic structure in the spinal ferrites generally follows the two sub-lattice pattern of ferrimagnetism of the Neel, in which the resultant magnetization is the disparity between B-site and A-site magnetization ensures that they are collinear and antiparallel to each other. Among all the three interactions (A-A, A-B and B-B) A-B interaction is efficient and powerful, it aligns the magnetic spins of the A site to the B site, so the net magnetic moment of the lattice is the difference between the B and A sub lattices, i.e. $M=|M_B–M_A|$. the addition of Zn ions forces the same number of Fe^{3+} ions from A- site to B-site as a result the magnetic moment of B-site increases, so magnetization and magnetic moment increase due to Zn2+. The hysteresis curves of the prepared nano ZFs by SCS, GCS and HYDS methods were measured at room and low temperatures over the field range -20,000 G to +20,000 G are as shown in Fig.4.1. The closure view of the hysteresis loops for the samples prepared by SCS method is shown in the Fig. 4.2 to know the exact values of Ms, Mr and Hc. The curves shape shows the ferrimagnetic nature with almost zero Hc.

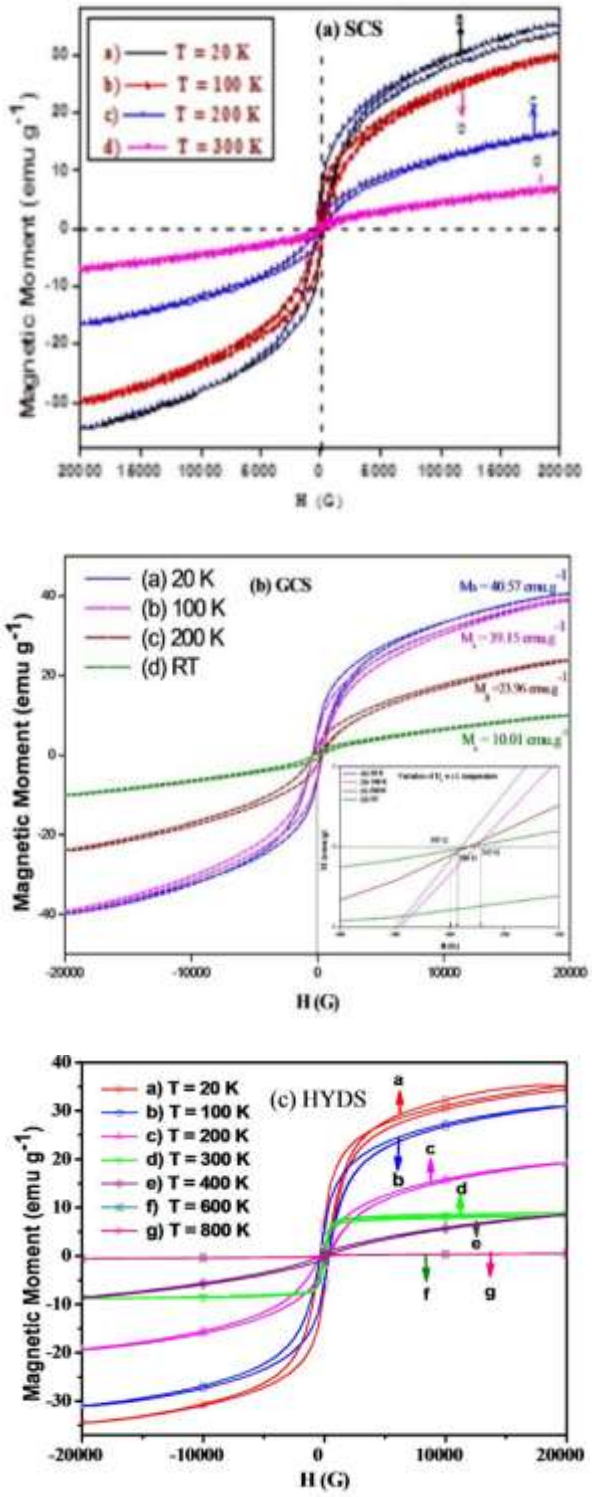

Fig. 4.1. The magnetic hysteresis of (a) SCS, (b) HYDS and (c) GCS samples of $ZnFe_2O_4$, studied at various low temperatures.

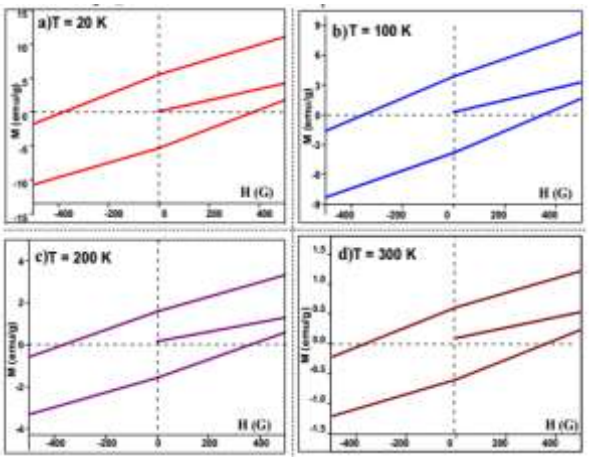

Fig.4.2. The close view of hysteresis curves to estimate the coercivity and retentivity values at (A) 20 K, (b) 100 K (c) 200 K and (d) 300 K for ZF obtained by SCS.

The magnetic properties like Ms, Mr, (Mr/Ms), Hc, magnetic moment (nB), Yafet-Kittel angles {α(y-k)} and superparamagnetic time of interaction at different temperatures varying from 20 - 800 K are reported.

The magnetic moment nB is calculated from hysteresis data by using the relation [212].

$$n_B = \left\{ \frac{M}{N_A \mu_{GB}} \right\} M_S \quad \text{.....[5.1]}$$

Where M is the molecular weight of the samples, M_S is the saturation magnetization, N is the Avogadro's number and is the Bohr magneton. On the basis of Neel's two-sublattice model, the Y-K angles are calculated using relation.

$$\cos \alpha_{YK} = \frac{n_B + M_A}{M_B} \quad \text{.....[5.2]}$$

The presence of canted spin gives rise to Y_K angle which compares the strength of A-B and B-B interactions [213]. The (Mr/Ms) and HC values suggest the existence of single domain (SD) particles in the sample [214]. The cubic magneto crystalline anisotropy or magnetic anisotropy energy density k was determined by using the law of approach to the Ms. The law of approach is valid in the range of 0.96 Ms < M < Ms therefore, the high field region of the magnetization curve where 0.96 Ms < M < Ms was valid is used to determine 'k' [215].

$$k = \frac{(M_S \times H_S)}{0.96} \quad \text{.....[5.3]}$$

In general, at a given temperature, below a certain critical size most of the magnetic materials show a phenomenon of superparamagnetic also called sudden magnetic flipping state. For the particles

with uniaxial magnetic anisotropy, the superparamagnetic relaxation as a result of thermal fluctuation is given by [216, 217]

Where

$$\tau_0 \frac{\tau}{\tau_0} = e^{\frac{kv}{k_B T}} \quad \text{.....[5.4]}$$

is called the attempt period an intrinsic property of the material; its value is 10-9 to 10-10 s, 'k_B' is Boltzmann constant, V is the volume of the unit cell and T is the absolute temperature. The ratio of (τ/τ_0) is less than one leading to superparamagnetic state. For all the samples prepared by SCS, GCS and HYDS methods, the crystallite sizes were in the nano range and slightly agglomerated, hence these mixtures showed a coexistence of superparamagnetic and ferrimagnetic state.

The reduction of 'M_s' and (τ/τ_0) is majorly due to thermal effects and in addition the spins canted on the surface of the nanoparticles loses the balance exchange interactions of the magnetic ions. Since the value of (τ/τ_0) is very close to one at 300 K shows the more of superparamagnetic nature than the ferrimagnetic. Temperature dependence of magnetization under both zero-field-cooled (ZFC) and field cooled (FC) conditions for ZFs obtained by SCS, GCS and HYDS were shown in Fig.5.3. ZFC curves were obtained by cooling the sample from RT to 20 K in absence of external magnetic field. In the case of FC, in the presence of 100 G magnetic field the variation of magnetization was recorded as a function of temperature. There is a gradual increase in temperature and ZFC curves exhibits a broad cusp and achieves maximum at blocking temperature TB. The width of the cusp in ZFC curve indicates the existence of particles with different sizes. Fig.5.3 shows that the TB for the samples prepared by SCS seems to be above RT but for GCS and HYDS samples, the TB values were 257 K and 293 K respectively. The relatively larger TB may be due to the significant contributions to anisotropy in the sample. The branches ZFC and FC reveal a temperature dependency, which is a result of aggregation effects arising from dipolar interactions. The aggregations observed in the SEM images supports for the same. It is found that the variation of ZFC curve shows the similar trend as the 100 G field FC curve. The divergence between MZFC and MFC was observed at much lower temperature called spin freezing temperature (Tf) where the spin freezing state or RSG appears. The ZFC and FC branches show a temperature dependency, which is a consequence of aggregation effects resulting from dipolar interactions [218-220].

The peak values of MZFC and MFC are 2.71 and 3.02 emu.g-1 for samples of SCS, 13.29 and 20.5 emu.g-1 for samples of GCS and 3.24 and 3.56 emu.g-1 for HYDS samples at Tf = 30K. The small cusps in the ZFC-FC curves in the range of 80-100 K, supports for the super paramagnetic TB but this cusp was not observed in GCS method shows that the samples of this method are more of ferrimagnetic in nature at low temperature. Nonetheless, an exact form of interaction can only be verified with field-dependent tests of the ZFC-FC or AC susceptibility tests. The ZFC and FC divisions show a temperature dependency resulting from the effects of dipolar interactions or aggregations. The dipolar interactions are confirmed by the agglomerations found in the SEM micrographs and the force constant values obtained from FTIR spectra.

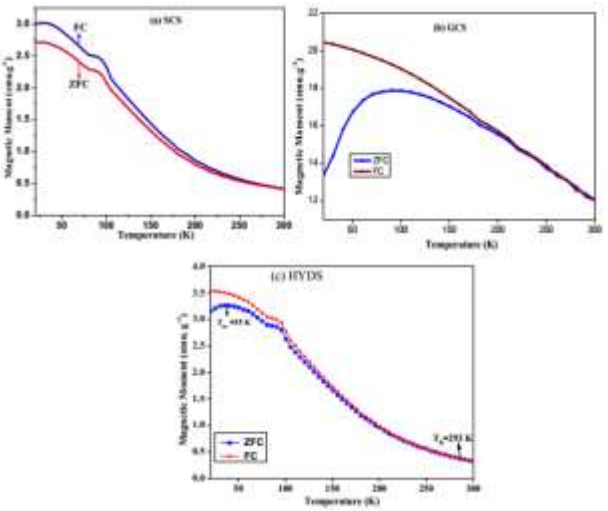

Fig.4.3. ZFC and FC curves from 20 K to 300 K shows the TB and Tirr (a) SCS (b) GCS and (c) HYDS samples.

Figs., 4.4 and 4.5 shows the ferrimagnetic behaviour at RT for all the Cr^{3+} doped samples obtained by SCS, GCS and HYDS methods. The values of Ms, Hc and Mr were decreased with increase in Cr^{3+} ions. The decrease in magnetization with Cr content was due to the dilution of magnetization of B- sublattice by Cr^{3+} ions.

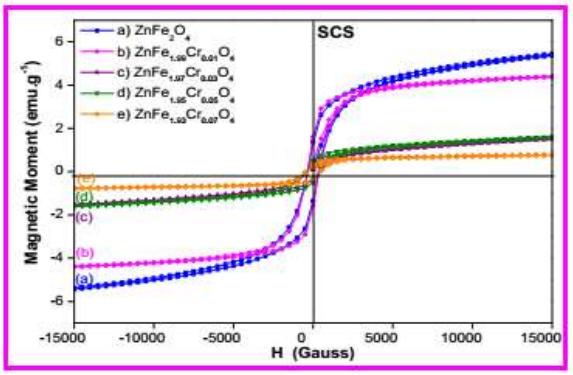

Fig.4.4. Hysteresis loops of ZnFe2-xCrxO4 (x=0.01 – 0.07) prepared using the method of GCS.

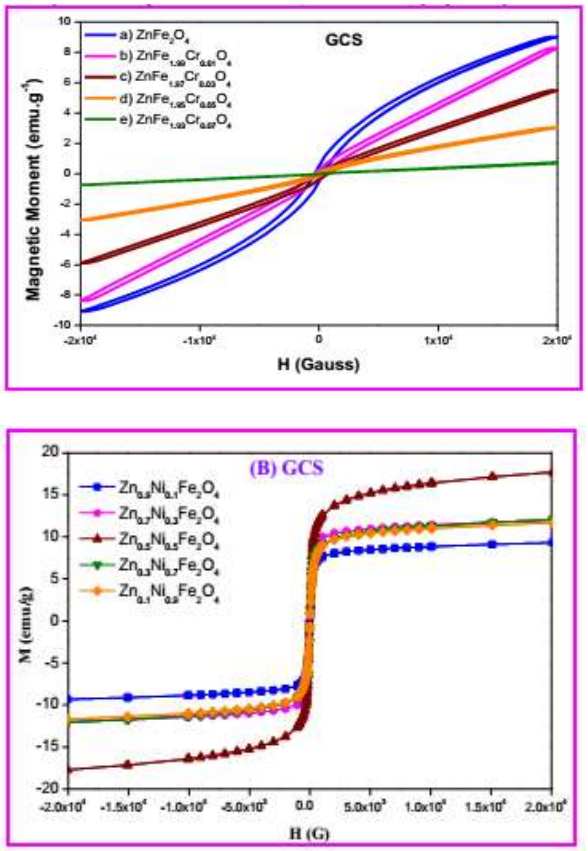

Fig.4.5. Hysteresis loops of ZnFe2-xCrxO4 (x=0.01 – 0.07) prepared using the method of HYDS

A decrease in Ms is expected when Cr^{3+} ions were added to the ferrite lattice as observed in previous reports attributable to the weakness of the Cr-ZF system's magnetic interactions. The variation of coercivity depends on the various factors namely magnetocrystallinity, microstrain, morphology and size distribution, magnetic domain size, anisotropy etc. [221, 222]. The development of additional phase at the grain boundaries breaks the microstructure and increases the localized distortion in the internal grain area resulting in reduced internal stress resulting in a small increase in coercion with Cr3 + ions. The grain boundary increase with an increase in Cr3 + ions was due to a decrease in crystallite thickness. The region of disordered arrangement for atoms on grain boundaries will fix and impede the movement of domain walls, hence the sample Hc increases slightly with Cr^{3+} content increase. The content of the Cr3 + ions of the earlier reports was far higher than that of the present material. This was therefore able to tune the magnetic properties with much smaller concentration of chromium ions within the ZF NPs. Fe^{3+} ions were replaced by Cr^{3+} ions having low magnetic moment resulting the decrease in net nB of the composition.

At RT, which is a measure of their magneto-crystalline anisotropy, the Hc of the samples has found very high. Such samples therefore support their use in high frequency transformers [223-225].

Another important soft ferrite is Ni-ZF, which shows potential applications in electromagnetic devices such as DC-DC converts, noise suppressors of EM waves, inductors, H_2 and H_2S gas sensing [226-228]. The RT magnetic properties of Ni-ZF prepared by SCS and GCS methods were shown in Fig. 4.6. In both the methods, the Hc value was very low. The Ms, nB, Hc and Mr of Ni-ZF prepared by both the methods.

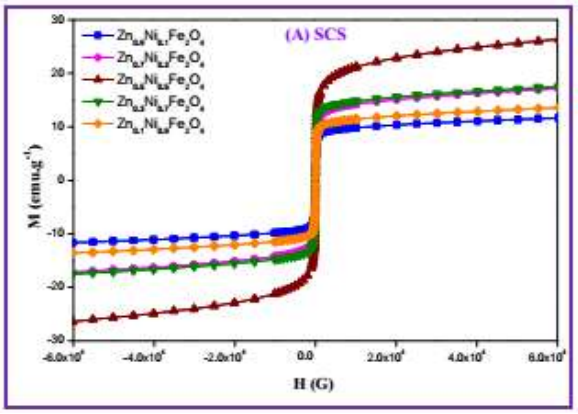

Fig.4.6. Hysteresis loops of Zn1-xNixFe$_2$O$_4$ (x=0.1 – 0.9) prepared using the method of (A) SCS and (B) GCS

ZFs doped with copper ions are important materials used in radio frequency circuits, high quality EM filters and high speed digital tapes. These are preferred more than the NiZF ferrites because of the carcinogenic effects of nickel and their environmental hazards [229 – 231]. Till the date NiZF are used because they possess high permeability and high resistivity at higher frequencies. So, to replace the use of Ni, the Cu was considered as an alternative system where the aim is to achieve the similar properties of NiZFs. Further, multilayer chip inductor (MLIC) applications where metallic silver is used as internal electrode material which has melting point of 961°C. Hence technologically, NiZF or CuZF or NiCuZFs were preferred as better magnetic material for MLIC is because of their lower densification temperatures and better performance at high frequencies [232].

Fig. 4.7 shows narrow loops with a behaviour characteristic of soft magnetic materials Ms value increases linearly with increasing in Cu content up to x = 0.6 followed by a remarkable decrease after this composition. The variation in Ms can be explained on the basis of cation distribution and the exchange interaction between *A* & *B* sites respectively. Cu^{2+} ions with magnetic moment of 1 B preferentially tend to migrate to the B-sites by replacing nonmagnetic Zn^{2+} ions with 0B which have a stronger preference for the *A*-site. Therefore Zn^{2+} displaces Fe^{3+} from site A to site B and enhances the magnetization of these sublattice sites by Cu^{2+} ions in B- sites. Since the magnetic spin of the neighboring A and B sites is anti-

www.ignited.in

ferromagnetically coupled due to the super-exchange interaction in the ferrite lattice, the net effect is an increase in the magnetic moment on the B- sublattice and thus the net moment of the spinel ferrite increases with Cu^{2+} ions as shown in Fig. 4.7.

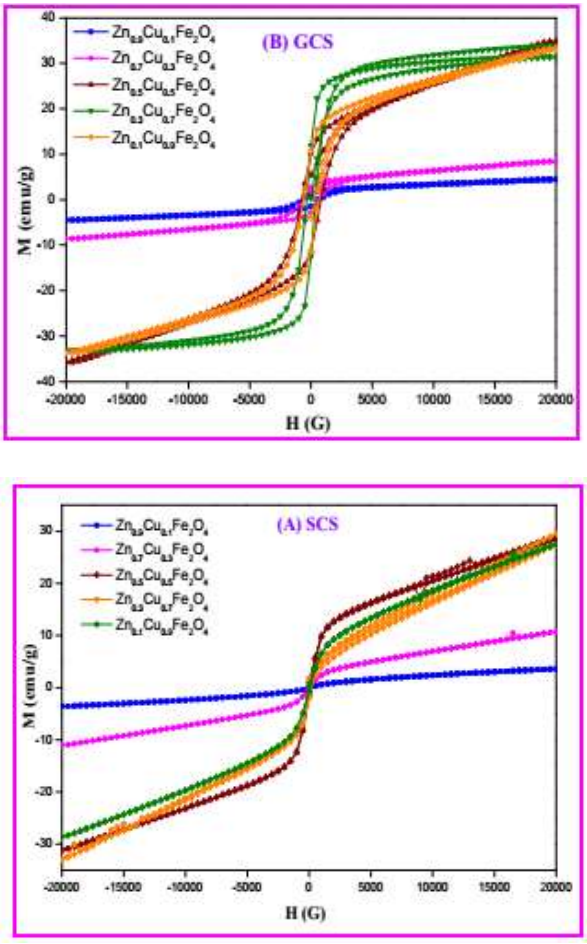

Fig.4.7. Hysteresis loops of $Zn_{1-x}NixFe_2O_4$ (x=0.1 – 0.9) prepared using the method of (A) SCS and (B) GCS

5. CONCLUSIONS

This study deals with principle and brief description of the theory of magnetization, experimental techniques used for magnetic properties for the samples synthesized by the three methods of preparation. Cr3+, Ni2+ and Cu2+ ions were incorporated into nano ZFs synthesized by both SCS and GCS methods. Compared with other methods of preparation, the mixed behaviour of superparamagnetic and ferrimagnetic behaviors were observed for nano ZF compounds with moderate grain sizes. Hence along with the size, the preparation procedure is also an important factor resulting in nearly to superparamagnetism of ZF nanoparticles at RT to up to 100 K. The values of saturation magnetization (Ms), coercivity (Hc) and retentivity (Mr) were changed with increase in dopant ions. The variation of Hc depends on the factors such as magnetocrystallinity, microstrain, morphology of magnetic particle and size distribution, magnetic domain size and anisotropy. In nano ZF compounds, due to non-magnetic substitution, intra-sublattice interaction is comparable with inter-sublattice interaction hence the disordered and frustration in the spin subsystem lead to the mechanisms of ferrimagnetic / antiferromagnetic order, local spin canting and re-entrant spin glass (*RSG*) were observed. The value of spin relaxation time in magnetic state of the samples was found to be nearly equal to one at 300 K confirms the perfect superparamagnetic property of *ZF*.

6. REFERENCES

1. M. A. Meyers, A. Mishra, D. J. Benson (2006). Mechanical Properties of nanocrystalline materials, Prog. Mater. Sci. 51, pp. 427 – 456.

2. C. Fenselau (2015). The 2015 Annual Review Issue, Anal. Chem.. 87, pp. 1-2.

3. C. Brechignac, P. Houdy, M. Lahmani (2007). Nanomaterials and nanochemistry, Springer-Verlag, Belin, Heidelberg, New York.

4. K. Thorkelsson, P. Bai, T. Xu (2015). Self-assembly and applications of anisotropic nanomaterials: A review, Nanotoday, 10, pp. 48-66.

5. T. Hyeon, L. Manna, S. S. Wong (2015). Sustainable nanotechnology, Chem. Soc. Rev., 44, pp. 5755-5757.

6. J. L. Liu, S. Bashir (2015). Advanced nanomaterials and their applications in renewable energy, Elsevier, Waltham, MA, USA.

7. R. Krahne, G. Morello, A. Figuerola, C. George, S. Deka, L. Manna (2011). Physical properties of elongated inorganic nanoparticles, Phys. Rep., 501, pp. 75-221.

8. M. Kuno (2012). Introductory nanoscience: Physical and chemical concepts, MRS Bulletin, 37, pp. 169- 170.

9. L. Zhang, M. Fang (2010). Nanomaterials in pollution trace detection and environmental improvement, Nanotoday, 5, pp. 128-142.

10. D. Kedem, T. Rothem (1967). Internal fields in nickel ferrite, Phys. Rev. Lett. 18, pp. 165 – 166.

11. C. G. Koops (1951). On dispersion of resistivity and dielectric constant of some

semiconductors at audiofrequencies, Phys. Rev. 83, pp. 121-124.

12. J. H. Rowen, E. F. Kankowski (1956). Dielectric properties of and conductivity in ferrites, Proc. IRE 44, pp. 1294 – 1303.

13. N. S. S. Murthy, M. G. Natera, S. I. Youssef, R. J. Begum, C. M. Srivastava (1969). Yafet-Kittel angles in zinc-nickel ferrites, Phys. Rew. 181, pp. 969 – 977.

14. A. E. Berkowitz, J. A. Lahut, I. S. Jacobs, L. M. Levinson (1975). Spin pinning at ferrite-organic interfaces, Phys. Rev. Lett. 34, pp. 594–597.

15. G. C. Jain, K. B. Das, R. B. Tripathi, R. Narayan (1982). Influence of V2O5 on magnetic peoperties of Ni-Zn ferrites, IEEE Trans. Magn. MAG-18, pp. 776- 778.

Corresponding Author

Mohammad Suhel*

Research Scholar, Department of Physics, Sri Satya Sai University of Technology & Medical Sciences, Sehore, M.P., Sehore